

# Zn<sup>2+</sup>-Aβ<sub>40</sub> Complexes Form Metastable Quasi-spherical Oligomers That Are Cytotoxic to Cultured Hippocampal Neurons<sup>\*[S]</sup>

Received for publication, January 18, 2012, and in revised form, April 19, 2012. Published, JBC Papers in Press, April 23, 2012, DOI 10.1074/jbc.M112.344036

Inna Solomonov<sup>‡S1</sup>, Eduard Korkotian<sup>¶1</sup>, Benjamin Born<sup>‡S</sup>, Yishay Feldman<sup>||</sup>, Arkady Bitler<sup>||</sup>, Farid Rahimi<sup>\*\*</sup>, Huiyuan Li<sup>\*\*</sup>, Gal Bitan<sup>\*\*\*SS</sup>, and Irit Sagi<sup>‡S2,3</sup>

From the <sup>‡</sup>Department of Structural Biology, <sup>S</sup>Department of Biological Regulation, <sup>¶</sup>Department of Neurobiology, and <sup>||</sup>Department of Chemical Research Support, the Weizmann Institute of Science, Rehovot 76100, Israel, the <sup>\*\*</sup>Department of Neurology, David Geffen School of Medicine, <sup>††</sup>Brain Research Institute, and <sup>SS</sup>Molecular Biology Institute, University of California at Los Angeles, Los Angeles, California 90095

**Background:** The mechanism by which interaction between Aβ and Zn<sup>2+</sup> induces Aβ aggregation and cell toxicity is elusive.

**Results:** Zn<sup>2+</sup> and Aβ<sub>40</sub> form metastable neurotoxic oligomers.

**Conclusion:** Aβ<sub>40</sub> binding to Zn<sup>2+</sup> leads to formation of small neurotoxic oligomers that become benign upon further self-assembly.

**Significance:** We provide a structure-function analysis of Zn<sup>2+</sup>-stabilized Aβ<sub>40</sub>, a neurotoxic species that may contribute to the pathology in AD.

The roles of metal ions in promoting amyloid β-protein (Aβ) oligomerization associated with Alzheimer disease are increasingly recognized. However, the detailed structures dictating toxicity remain elusive for Aβ oligomers stabilized by metal ions. Here, we show that small Zn<sup>2+</sup>-bound Aβ<sub>1–40</sub> (Zn<sup>2+</sup>-Aβ<sub>40</sub>) oligomers formed in cell culture medium exhibit quasi-spherical structures similar to native amylospheroids isolated recently from Alzheimer disease patients. These quasi-spherical Zn<sup>2+</sup>-Aβ<sub>40</sub> oligomers irreversibly inhibit spontaneous neuronal activity and cause massive cell death in primary hippocampal neurons. Spectroscopic and x-ray diffraction structural analyses indicate that despite their non-fibrillar morphology, the metastable Zn<sup>2+</sup>-Aβ<sub>40</sub> oligomers are rich in β-sheet and cross-β structures. Thus, Zn<sup>2+</sup> promotes Aβ<sub>40</sub> neurotoxicity by structural organization mechanisms mediated by coordination chemistry.

The predominant proteinaceous component of amyloid plaques, a pathological hallmark of Alzheimer disease (AD)<sup>4</sup>, is amyloid β-protein (Aβ). Aβ is generated by sequential enzy-

matic cleavage of the amyloid β-protein precursor (APP) by β- and γ-secretases (1). The two major forms of Aβ produced from APP contain 40 (Aβ<sub>40</sub>) or 42 (Aβ<sub>42</sub>) amino acid residues. The cause of AD is believed to be pathological accumulation and self-association of Aβ into neurotoxic oligomers. These impair synaptic communication and trigger a cascade of events, leading to neurodegeneration in susceptible brain areas (2, 3). Aβ oligomers, rather than Aβ fibrils, are considered the primary neurotoxic agents acting in AD (4, 5).

Various factors and events that modulate Aβ toxicity include disruption of metal homeostasis, disruption of critical metabolic processes, inflammation, and oxidative stress. These factors make working in this field extremely challenging; in particular, elucidating the molecular mechanisms governing the pathology of Aβ misfolding and aggregation. For example, Zn<sup>2+</sup> is highly enriched in AD plaques compared with healthy, aged-matched brain tissues (6–9). Certain neurons in the mammalian cerebral cortices store up to millimolar Zn<sup>2+</sup> concentrations and release Zn<sup>2+</sup> in (sub)millimolar pulses from their presynaptic terminals (10). Synaptic Zn<sup>2+</sup> may play a critical role in mediating toxicity induced by Aβ oligomers (11). Specifically, transgenic mouse models of AD demonstrated significantly reduced loads of cerebral senile plaques and precipitated Aβ when the gene for the synaptic vesicle transporter ZnT3 (*SLC30A3*) was knocked out (12). *In vitro*, Zn<sup>2+</sup> interacts with Aβ<sub>40</sub>, inducing its aggregation within milliseconds (13, 14). It was shown that Zn<sup>2+</sup> interacts with soluble Aβ<sub>40</sub> oligomers and alters their stability (15). Importantly, physiological conditions, such as the presence of NaCl, significantly accelerate Zn<sup>2+</sup>-induced Aβ aggregation (16). The rapid interaction of Zn<sup>2+</sup> with Aβ<sub>40</sub> results in formation of quasi-spherical aggregates. With aging, these aggregates increase in size significantly

<sup>\*</sup> This work was supported in part by National Institutes of Health Grants AG027818 (to G. B.) and CA098799 (to I. Sagi). This work was also supported by United States-Israel Binational Science Foundation Grant 2007187 (to G. B. and I. Sagi), by a Human Frontier Science Program cross-disciplinary fellowship and a Dean of Faculty fellowship of the Weizmann Institute (to B. B.), and by the Israel Science Foundation, the Kimmelman Center at the Weizmann Institute, and the Ambach family fund (to I. Sagi).

<sup>[S]</sup> This article contains supplemental Figs. S1–S6.

<sup>1</sup> Both authors contributed equally to this work.

<sup>2</sup> To whom correspondence should be addressed: Department of Structural Biology and Department of Biological Regulation, The Weizmann Institute of Science, Rehovot 76100, Israel. Tel.: 972-8934-2130; Fax: 972-8934-4116; E-mail: irit.sagi@weizmann.ac.il.

<sup>3</sup> Incumbent of the Pontecorvo Professorial Chair.

<sup>4</sup> The abbreviations used are: AD, Alzheimer disease; Aβ, amyloid β-protein; APP, amyloid β-protein precursor; TEM, transmission electron microscopy;

AFM, atomic force microscopy; ThT, thioflavin T; MEM, minimal essential medium; HS, horse serum.

and do not convert into fibrils (17). Interaction of Zn<sup>2+</sup> with Aβ40 increases the exposure of hydrophobic surfaces in Aβ40 (18).

Zn<sup>2+</sup>-induced Aβ aggregates were proposed as neurotoxic agents disrupting synaptic communication (11, 13). However, the molecular determinants driving neurotoxicity remain elusive. We thus set out to perform a detailed structure-toxicity analyses of Aβ40 in the presence of Zn<sup>2+</sup> in serum-free culture media. Here, we report the self-assembly pathways and structure-toxicity interplay of Zn<sup>2+</sup>-induced, quasi-spherical metastable Aβ40 oligomers (Zn<sup>2+</sup>-Aβ40). These oligomers possess conformational characteristics typical of fibrillar structures, yet their morphology is non-fibrillar. They irreversibly affect spontaneous calcium activity and neuron viability.

## EXPERIMENTAL PROCEDURES

**Reagents**—All reagents were purchased from Sigma-Aldrich (Israel) unless mentioned otherwise. All reagents were of analytical grade. Purified deionized water was prepared using a Milli-Q water-purification system (Millipore, Billerica, MA).

**Aβ40 Sample Preparation**—Aβ40 was purchased from rPep-tide and prepared for experiments as described previously (14). Briefly, Aβ40 was dissolved at 665 μM (defined by UV-Vis spectroscopy with ε<sub>292</sub> = 2300 M<sup>-1</sup> cm<sup>-1</sup>) in 10 mM NaOH, sonicated for 1 min in a Branson 1510 bath sonicator, and centrifuged for 10 min at 12,000 × g at 4 °C to precipitate large aggregates. Concentrations of stock solutions prepared this way were occasionally confirmed by amino acid analysis. The differences in the concentrations determined by absorption and amino acid analysis were < 8%. The stock solutions were diluted to 230 μM in 10 mM MOPS (pH 6.9 ± 0.1). These solutions did not scatter near-UV light at 300 nm, suggesting that they did not contain large aggregates or fibrils. Moreover, Aβ40 preparations were hardly distinguishable from the control (buffer) by transmission electron microscopy (TEM) examination at *t* = 0 (supplemental Fig. S1a). In such preparations, Aβ40 monomers coexist with low-molecular-weight oligomers (19). Zn<sup>2+</sup>-Aβ40 oligomers were prepared by adding 0.01 M ZnCl<sub>2</sub> (in 10 mM MOPS) to the Aβ40 solution. For fibril preparation, 230 μM Aβ40 was incubated for 7 days at 37 °C without agitation. Fibril formation was examined by TEM (supplemental Fig. S2).

In TEM, atomic force microscopy (AFM), CD, thioflavin T (ThT) fluorescence, and cell-culture experiments, the final Aβ40 and Zn<sup>2+</sup> concentrations were 10 and 20 μM, respectively (Aβ concentration calculated for the monomeric protein). We estimated the concentration of free Zn<sup>2+</sup> in our preparations by using data published by Bush *et al.* (13), assuming two binding sites for Zn<sup>2+</sup> on Aβ:

$$B = (R1 \times L_F)/(K_{d1} + L_F) + (R2 \times L_F)/(K_{d2} + L_F) \quad (\text{Eq. 1})$$

where *B* is the concentration of Zn<sup>2+</sup>-Aβ40 oligomers, *L<sub>F</sub>* is the concentration of free Zn<sup>2+</sup>, *R1* and *R2* are the concentrations of each Zn<sup>2+</sup>-binding site, and *K<sub>d1</sub>* and *K<sub>d2</sub>* are the respective dissociation constants.

Accordingly, the concentration of free Zn<sup>2+</sup> in our preparations is estimated at 5.15 μM. These calculations suggest that

under the conditions we used, each Aβ40 molecule binds ~ 1.5 Zn<sup>2+</sup> ions.

TEM, AFM, CD, and ThT experiments were performed in serum-free cell-culture medium (129 mM NaCl, 4 mM KCl, 1 mM MgCl<sub>2</sub>, 2 mM CaCl<sub>2</sub>, 10 mM glucose, and 10 mM HEPES (pH 7.4) with osmolarity adjusted to 320 mOsm) using dilutions identical to those used in cell culture experiments. Fibril suspensions in MOPS were sonicated for 20 s, centrifuged for 20 min at 2000 × g, washed three times in 10 mM MOPS, and finally added to neuronal cultures. All morphologies were prepared in MOPS and comprised 8.7% of the final volume of culture medium.

**Electron Microscopy**—Images were acquired using a Tecnai 12 transmission electron microscope (FEI, Eindhoven, The Netherlands) operated at 120 kV. Micrographs were taken using a MegaView III charge-coupled device camera (SIS, Münster, Germany). Aliquots of different Aβ40 preparations were adsorbed for 1 min onto carbon-coated copper grids and negatively stained with 1% (w/v) uranyl acetate for 30 s. TEM images were analyzed using ImageJ.

**Atomic Force Microscopy**—Aliquots (5 μl) of freshly prepared Zn<sup>2+</sup>-Aβ40 were spotted onto freshly cleaved mica (Ted Pella, Inc., Redding, CA), incubated at room temperature for 3 min, rinsed with Milli-Q water, and air-dried. At least five different regions on the mica surface were examined.

Images were collected using a MultiMode AFM with a Nano-scope V controller (Veeco Metrology LLC, Santa Barbara, CA) equipped with an *E*-scanner in tapping mode at 22–24 °C. All images were recorded using silicon microcantilevers (OMCL-AC240TS-W2, Olympus) with a spring constant of ~2 N/m (manufacturer-specified) and at a scan rate of 1–3 Hz. The target amplitude was 300 mV with a set point of ~230 mV for all measurements. Images were acquired in different scan directions and at different scales to verify the consistency of the evaluated structures.

Profiles of Zn<sup>2+</sup>-Aβ40 oligomers were acquired from the AFM images, and the corresponding aggregate heights were calculated, binned, normalized, and plotted using Matlab (MathWorks, Inc., Natick, MA).

**Circular Dichroism Spectroscopy**—Room-temperature CD spectra of 10 μM Zn<sup>2+</sup>-free Aβ40 or Zn<sup>2+</sup>-Aβ40 solutions in serum-free media were measured at *t* = 0 h and *t* = 2 h in 2-mm path-length quartz cuvettes (Helma, Jena, Germany) in the spectral range of 200–260 nm. Spectra were recorded using a JASCO 815 spectropolarimeter at a 100-nm/min scan rate with 0.2-nm resolution. For each sample, four spectra were acquired and averaged. The background was subtracted, and the spectra were smoothed using OriginPro 8.0.

**X-ray Powder Diffraction**—MOPS stock solutions containing Zn<sup>2+</sup>-Aβ40 were centrifuged at 12,000 × g for 10 min at 4 °C. The pellet was washed gently three times with 1 ml of Milli-Q water containing 1 μM ZnCl<sub>2</sub>, placed as a thick film onto a silicon zero-background sample holder, and air-dried for 30 min at room temperature. X-ray diffraction measurements were carried out in reflection mode using a TTRAX III θ-θ diffractometer (Rigaku, Japan) equipped with a rotating copper anode operating at 50 kV and 200 mA and a scintillation detector.

Parallel-beam optics (angle divergence  $\sim 0.05^\circ$ ) formed by a multilayered mirror (Rigaku, Cross Beam Optics attachment, Japan) were used to obtain high-quality data from a dried-drop sample at low diffraction angles. Specular diffraction ( $\theta/2\theta$  scan) was performed under ambient conditions from  $2^\circ$  to  $30^\circ$ . The average measurement time was  $\sim 5$  h. After 10 h, sample degradation was observed. The cross-section of the x-ray beam was  $1 \times 5 \text{ mm}^2$ , and the angular divergence of the reflected beam was limited to  $0.114^\circ$  by a parallel slit analyzer (PSA-80).

Peak positions and widths of the Bragg reflections were determined by a self-consistent profile-fitting procedure using Jade 9.1 (Materials Data, Inc., Livermore, CA). The coherent diffraction lengths observed in  $\text{Zn}^{2+}$ -A $\beta$ 40 were estimated by the Scherrer formula from the broadening of the corresponding peaks.

**ThT Fluorescence**—Triplicate 200- $\mu\text{L}$  samples were examined in plastic clear-bottom 96-well plates (Nunc 96F Maxi-sorp, Thermo Fisher Scientific, Roskilde, Denmark). The plates were incubated at  $25^\circ\text{C}$  for 72 h without agitation in a Synergy HT multi-mode microplate reader (Bio-Tek Instruments, Winooski, VT) with excitation and emission wavelengths/slit widths of 400 nm/30 nm and 485 nm/20 nm, respectively. To prevent evaporation, plates were tightly sealed with Parafilm (Plastic Packaging, Chicago, IL). The ThT fluorescence data were background-subtracted and plotted using OriginPro 8.0.

**Hippocampal Neuron Cultures**—Animal experiments were performed in accordance with the guidelines of the Institutional Animal Care and Use Committee of the Weizmann Institute and the Israeli national guidelines on animal care. Cell cultures were prepared as described previously (20). Briefly, rat pups were decapitated on the day of birth ( $P_0$ ), and their brains were removed and placed into Petri dishes containing chilled ( $4^\circ\text{C}$ ), oxygenated Leibovitz L15 medium (Invitrogen) supplemented with 0.6% glucose and gentamicin (20  $\mu\text{g}/\text{mL}$ , Sigma). Hippocampi were isolated, incubated with trypsin (0.25% w/v) and DNase (50  $\mu\text{g}/\text{mL}$ ), triturated, and then transferred to plating medium comprising 5% heat-inactivated horse serum (HS), 5% fetal bovine serum, and B-27 (1  $\mu\text{L}/\text{mL}$ ) prepared in minimum essential medium (MEM) (Invitrogen) supplemented with 0.6% glucose, 20  $\mu\text{g}/\text{mL}$  gentamicin, and 2 mM glutamax (enriched MEM).

Using 24-well plates,  $\sim 10^5$  hippocampal neurons were plated in 1 mL of medium/well onto a hippocampal glial cell feeder layer. The feeder layer was grown on poly-lysine-coated glass cover slips for 2 weeks before transferring the neurons. On day 3, the medium was changed to enriched MEM containing 10% HS and a mixture of 5'-fluoro-2-deoxyuridine/uridine (20  $\mu\text{g}/\text{mL}$  and 50  $\mu\text{g}/\text{mL}$ , respectively, Sigma) to block glial cell proliferation. On day 7, the medium was changed to MEM-containing 10% HS with no further modifications until cells were used for experiments.

**Intracellular  $\text{Ca}^{2+}$  Imaging**—Postnatal cultures 2–3 weeks after plating were used for  $\text{Ca}^{2+}$  imaging. First, cells were washed in serum-free cell-culture media containing 129 mM NaCl, 4 mM KCl, 1 mM  $\text{MgCl}_2$ , 2 mM  $\text{CaCl}_2$ , 10 mM glucose, and 10 mM HEPES (pH 7.4) with osmolarity adjusted to 320 mOsm.

Cells were incubated for 1 h at  $23^\circ\text{C}$  in the dark in the same serum-free media containing 2  $\mu\text{M}$  Fluo-4AM (Invitrogen/Molecular Probes). The cells were then extensively washed for 5 min and imaged using an upright Zeiss PASCAL confocal microscope with an Olympus  $\times 63$  water immersion lens (0.9 numerical aperture) and  $\times 1$ –2 scan zoom in bidirectional scan mode. Laser power, pinhole diameter, and detector gains were adjusted and standardized to avoid photo damage and pixel saturation. Each field was recorded for 5 min without signs of cellular photo toxicity or changes in spontaneous firing rates.

As all A $\beta$ 40 preparations initially were prepared in MOPS buffer, we tested their effects on the spontaneous activity of cultured neurons in 10 mM MOPS (pH  $6.9 \pm 0.1$ ). We found that MOPS, which served as a control, did not affect the rate or the amplitude of  $\text{Ca}^{2+}$  activity or  $[\text{Ca}^{2+}]_i$  ( $p > 0.05$ , Student's  $t$  test). Sequential images were taken at  $t = 0, 5, 30, 60, 90$ , and 120 min for each A $\beta$ 40 preparation, followed by a 30-min wash step.

**Cell Viability Analysis**—In initial experiments, we added 10  $\mu\text{M}$  of each A $\beta$ 40 preparation ( $\text{Zn}^{2+}$ -free A $\beta$ 40, A $\beta$ 40 fibrils or  $\text{Zn}^{2+}$ -A $\beta$ 40 oligomers), MOPS, or  $\text{Zn}^{2+}$  to hippocampal neurons and measured neuronal viability after 48 h incubation. The incubation conditions were serum-containing culture media (MEM containing 10% HS) at  $37^\circ\text{C}$  and 5%  $\text{CO}_2$ . Under these conditions, no toxicity was observed for any of the A $\beta$ 40 preparations. Comparison of  $\text{Zn}^{2+}$ -A $\beta$ 40 oligomers and control conditions is shown in supplemental Fig. S6.

In a modified protocol, four equal aliquots of  $\text{Zn}^{2+}$ -free A $\beta$ 40,  $\text{Zn}^{2+}$ -A $\beta$ 40 oligomers, or A $\beta$ 40 fibrils were added to primary hippocampal neurons every 12 h without changing the incubation conditions (1 mL MEM containing 10% HS at  $37^\circ\text{C}$ , 5%  $\text{CO}_2$ ). The final A $\beta$ 40 concentration was 10  $\mu\text{M}$  in each case. Cell survival was evaluated 72 h after the last application by assaying neuron-specific enolase or directly by phase-contrast microscopy.

**Immunocytochemistry**—Glass cover slips with treated cells were removed from the wells and washed briefly with the standard recording medium. The cells were fixed in 4% paraformaldehyde and 4% sucrose in 0.1 M PBS (pH 7.4) for 20 min and then washed thoroughly with PBS, incubated for 1 h in PBS containing 10% normal goat serum and 0.1% Triton X-100 to reduce nonspecific reactivity, and incubated with rabbit anti-neuron-specific enolase at  $4^\circ\text{C}$  for 24 h. The cells were then washed, incubated with Alexa Fluor 568-labeled caprine anti-rabbit secondary antibody (1:200, Molecular Probes, Eugene, OR) for 1 h, and washed. The coverslips were transferred onto glass slides and mounted in an anti-fading mounting medium comprising 90% glycerol and 0.1%  $p$ -phenylenediamine (Sigma) in 20 mM PBS (pH 8.5) for visualization. Confocal image stacks were recorded using a Zeiss LSM 510 laser-scanning microscope with a Zeiss  $\times 40$  oil-immersion objective (1.4 numerical aperture) and  $\times 1$  scan zoom. Detector gain and amplifier were initially set to obtain pixel densities within a linear range.

**Quantification, Statistics, and Digital Images**—Time lapse, immunostaining, and phase contrast images were analyzed using Zeiss LSM 510 or Zeiss PASCAL software (Carl Zeiss). The fluorescence signal was measured by producing regions of



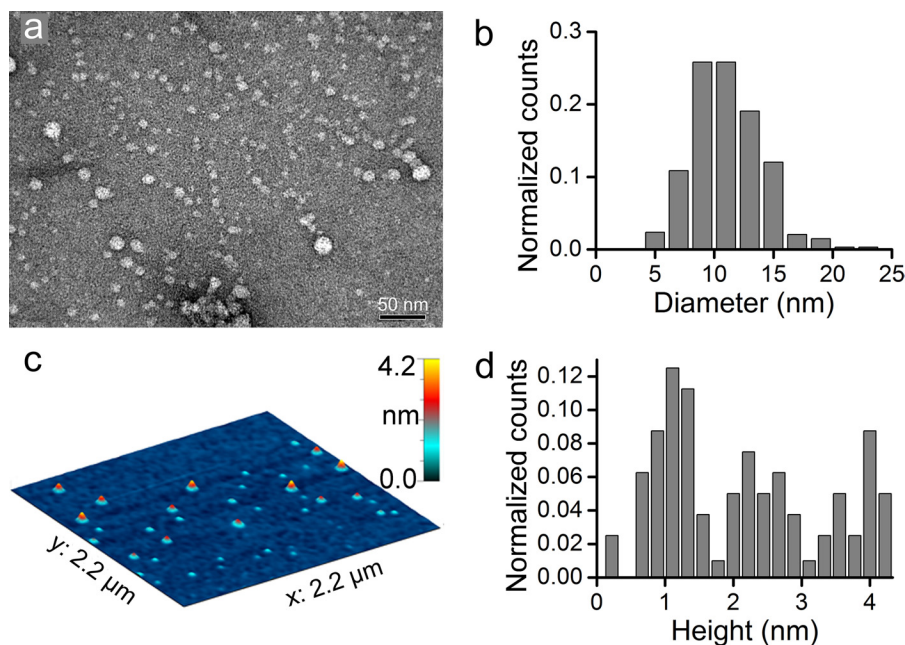


FIGURE 1. **Morphological characterization of freshly prepared metastable  $\text{Zn}^{2+}$ -A $\beta$ 40 oligomers in serum-free culture medium.** *a*, TEM image of  $\text{Zn}^{2+}$ -A $\beta$ 40. *b*, diameter distribution of  $\text{Zn}^{2+}$ -A $\beta$ 40 derived from TEM images. *c*, AFM image of  $\text{Zn}^{2+}$ -A $\beta$ 40 in air. *d*, height distribution of  $\text{Zn}^{2+}$ -A $\beta$ 40 derived from AFM images.

interest related to the shapes of cell bodies. Alternatively, profiles of fluorescence intensity were generated using ImageJ. Cells were measured and counted using a double-blinded procedure by an independent observer.  $[\text{Ca}^{2+}]_i$  events were counted automatically using a home-made Matlab program (The MathWorks, Inc., Asheboro, NC) and controlled manually.

Statistical analyses were performed by Student's *t* tests or analysis of variance using Matlab or KaleidaGraph (Synergy Software, Reading, PA). In each experiment, 4–6 cultures were used per group.

Figures were prepared using Photoshop CS2 (Adobe, San Jose, CA). Image brightness and contrast were adjusted uniformly across the entire image.

## RESULTS

**Morphology of  $\text{Zn}^{2+}$ -A $\beta$ 40 Oligomers in Serum-free Culture Media**—The rapid interaction of  $\text{Zn}^{2+}$  ions with A $\beta$ 40 induced aggregation mainly into quasi-spherical morphologies as observed previously in MOPS buffer (14). The experimental conditions used to assess A $\beta$  morphologies by TEM and AFM were similar to conditions used for neuron cultures. A $\beta$  morphologies were assessed at room temperature in serum-free culture media. Under these conditions, our preparations contained  $\sim 5 \mu\text{M}$  of unbound  $\text{Zn}^{2+}$ . In fresh  $\text{Zn}^{2+}$ -A $\beta$ 40 preparations, a distribution of predominantly quasi-spherical particles with 7–15-nm diameter was observed by TEM (Fig. 1, *a* and *b*). These  $\text{Zn}^{2+}$ -A $\beta$ 40 assemblies resembled those of toxic spherical oligomers of  $\text{Zn}^{2+}$ -free A $\beta$ 40 (22) stabilized at 4 °C for 30–60 h, although the latter had larger diameters (15–35 nm). The majority of the  $\text{Zn}^{2+}$ -A $\beta$ 40 complexes appeared to have stable size and morphology for at least 2 h at room temperature, whereas  $\sim 20\%$  of these structures increased in size after 2 h (supplemental Fig. S3). In contrast, the morphology and diam-

eter/length of structures observed in  $\text{Zn}^{2+}$ -free A $\beta$ 40 preparations (supplemental Fig. S1, *a* and *b*) increased substantially in the first 2 h of incubation. Thus, morphological changes in  $\text{Zn}^{2+}$ -free A $\beta$ 40 occur considerably faster than in  $\text{Zn}^{2+}$ -stabilized oligomers.

Height analyses of the  $\text{Zn}^{2+}$ -A $\beta$ 40 oligomers by AFM revealed distinct populations with heights of 1, 2, or 4 nm (Fig. 1, *c* and *d*). This suggests that aggregates are arranged in mono-, bi-, or tetralayers, assuming  $\sim 1$ -nm-thick monolayers within which A $\beta$ 40 molecules have a hairpin conformation (14).

Height-diameter correlation analysis of native neurotoxic amylophersoids (23) and  $\text{Zn}^{2+}$ -free cross-linked A $\beta$ 40 (24) yielded correlation coefficients of  $r^2 = 0.87$  and  $r^2 > 0.95$ , respectively. A similar height-diameter correlation analysis of  $\text{Zn}^{2+}$ -A $\beta$ 40 populations gave a correlation coefficient of  $r^2 = 0.055$ , demonstrating that heights and diameters were not correlated. Further analysis showed that the low correlation coefficient resulted from the existence of a relatively narrow population of diameters and three distinct populations of heights (Fig. 1, *b–d*). This suggests that  $\text{Zn}^{2+}$ -A $\beta$ 40 assembles in defined conformational protein blocks possessing an irregular structural organization in the horizontal plane and a regular organization in the vertical direction. This organization may be induced by stable hairpin conformation of A $\beta$ 40 and nonspecific intermolecular  $\text{Zn}^{2+}$  coordination (14, 25).

**Secondary and Tertiary Structures of  $\text{Zn}^{2+}$ -A $\beta$ 40**—The secondary and tertiary structures of  $\text{Zn}^{2+}$ -A $\beta$ 40 oligomers were analyzed by far-UV CD spectroscopy and x-ray powder diffraction (Fig. 2). At  $t = 0$ , the CD spectrum of  $\text{Zn}^{2+}$ -A $\beta$ 40 oligomers measured in serum-free media exhibited a minimum at 214 nm, indicating a high  $\beta$ -sheet content which was stable during 2 h of incubation at room temperature (Fig. 2*a*). Similar CD experiments assessing  $\text{Zn}^{2+}$ -free A $\beta$ 40 preparations at  $t =$

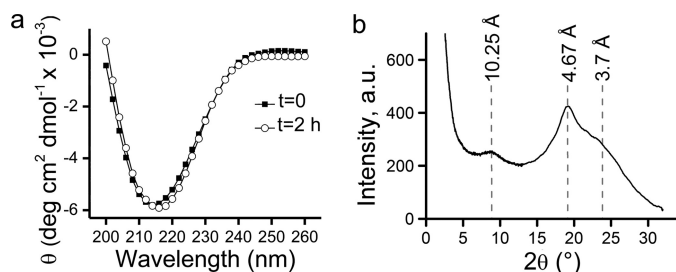


FIGURE 2. **Secondary and tertiary structure analyses of  $\text{Zn}^{2+}$ -A $\beta$ 40 oligomers in serum-free culture medium.** *a*, CD spectra of  $\text{Zn}^{2+}$ -A $\beta$ 40. *b*, x-ray powder diffraction pattern of  $\text{Zn}^{2+}$ -A $\beta$ 40. The intensity in *b* is given in arbitrary units (a.u.).

0 or  $t = 2$  h also showed the presence of  $\beta$ -sheets (supplemental Fig. S1c). Yet, the  $\beta$ -sheet content in these preparations increased substantially during the first 2 h of incubation, in agreement with the TEM data discussed above.

X-ray powder diffraction was used to elucidate the long-range order of metastable  $\text{Zn}^{2+}$ -A $\beta$ 40 oligomers (Fig. 2*b*). Fresh preparations of  $\text{Zn}^{2+}$ -A $\beta$ 40 in MOPS buffer were rapidly concentrated prior to x-ray measurements (see “Experimental Procedures”). The diffraction pattern collected in reflection mode exhibited three peaks with  $d$  spacings at 10.25, 4.67, and 3.7 Å, characteristic of amyloid fibrils (26–30) (Fig. 2*b*). This result was intriguing in view of the non-fibrillar, quasi-spherical morphology observed for the metastable  $\text{Zn}^{2+}$ -A $\beta$ 40 oligomers in both MOPS (14) and in serum-free culture media (Fig. 1). The most pronounced reflection peak corresponded to a distance of 4.67 Å and was attributed to intermolecular hydrogen bond distances. The coherence length of this reflection is  $\sim 20$  Å, corresponding to approximately four molecules of A $\beta$ 40 in a crystallite along the axis of hydrogen bonding. The reflection referring to 10.25 Å was attributed to the mean distance between peptides in neighboring sheets of A $\beta$ 40 molecules with a U-shaped hairpin conformation. This distance is in good agreement with the 1-nm height for monolayer arrangements of  $\text{Zn}^{2+}$ -A $\beta$ 40 oligomers measured by AFM (Fig. 1, *c* and *d*). The calculated coherence length for the 10.25 Å diffraction peak is  $\sim 42$  Å, corresponding to a tetra-layer of A $\beta$ 40, also in agreement with our AFM height analysis, which indicates a height of 4 nm (Fig. 1*d*). The low-intensity, broad reflection peak ( $> 6$ ) corresponding to  $\sim 3.7$  Å indicates a low degree of order of the pleated  $\beta$ -sheets. Similar peaks were observed in fibrils of glucagon (3.77 Å) (26), A $\beta$ 1–28 (3.8 Å) (27), and A $\beta$ 40 (3.8 Å) (28) and was interpreted by Glenner *et al.* (26) as average spacing between  $\text{C}_\alpha$  atoms in neighboring polypeptide chains. Our CD and x-ray powder diffraction data indicate that binding of  $\text{Zn}^{2+}$  to A $\beta$ 40 peptide does not interfere with the hairpin conformation observed in A $\beta$ 40 fibrils yet induces non-fibrillar morphologies, possibly via intermolecular  $\text{Zn}^{2+}$  coordination.

**Seeding A $\beta$ 40 with  $\text{Zn}^{2+}$ -A $\beta$ 40 Oligomers Inhibits Fibril Growth**—Our results indicate that  $\text{Zn}^{2+}$ -A $\beta$ 40 oligomers possess structural characteristics similar to those found in fibrils but do not have fibrillar morphology (14, 17, 18). To explore the overall effect of  $\text{Zn}^{2+}$ -A $\beta$ 40 oligomers on A $\beta$ 40 fibril formation, we analyzed their nucleation power by conducting time-dependent ThT fluorescence experiments in serum-free media. The ThT fluorescence assay quantitatively measures formation

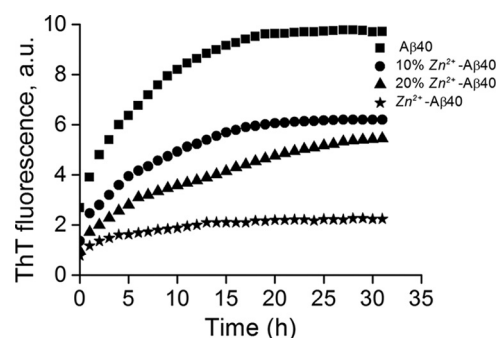
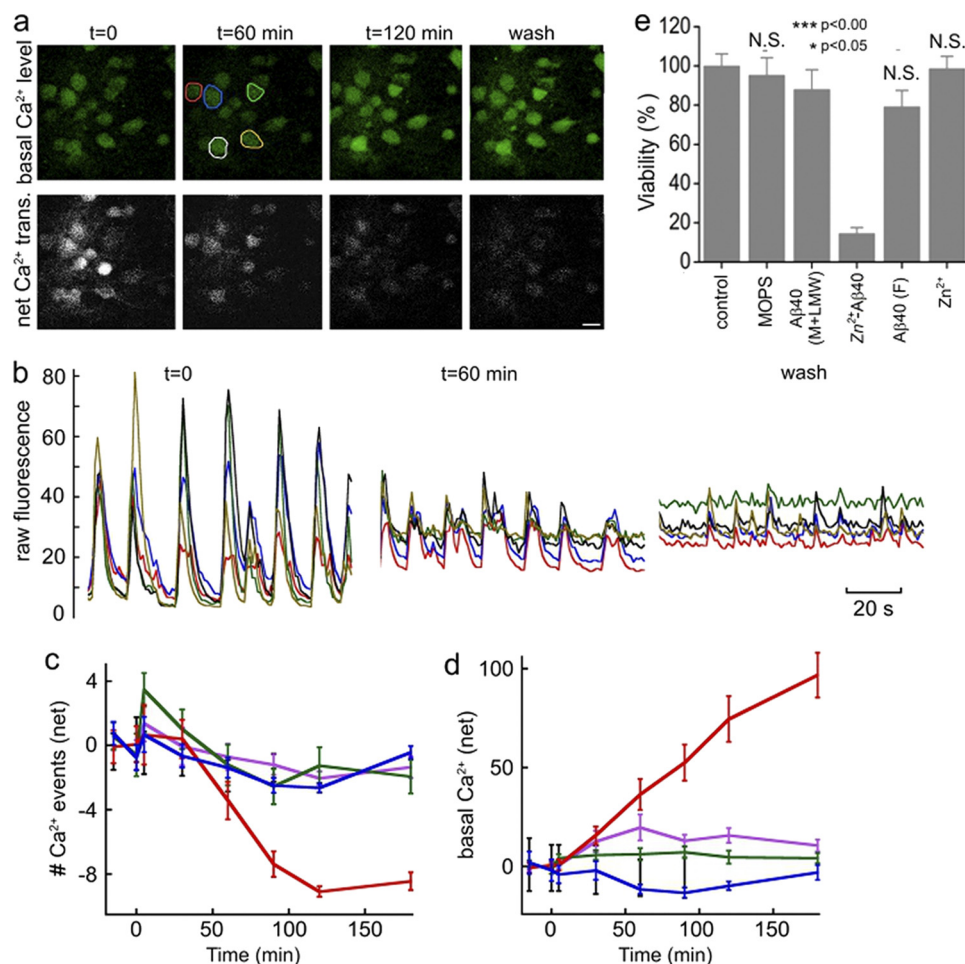


FIGURE 3. **Effects of metastable  $\text{Zn}^{2+}$ -A $\beta$ 40 oligomers on A $\beta$ 40 nucleation and fibril formation.**  $\beta$ -sheet formation was assessed in solutions of 10  $\mu\text{M}$   $\text{Zn}^{2+}$ -free A $\beta$ 40, 10  $\mu\text{M}$   $\text{Zn}^{2+}$ -A $\beta$ 40 oligomers, or mixtures of these two preparations at 9:1 or 4:1 concentration ratios, respectively, by measuring the change in ThT fluorescence over time. ThT fluorescence is given in arbitrary units (a.u.).

of cross- $\beta$ -sheet structures (31) and is commonly used for monitoring A $\beta$  assembly kinetics (32). The ThT fluorescence signal was recorded over 72 h at 25 °C without agitation in  $\text{Zn}^{2+}$ -free A $\beta$ 40 (comprising monomers and low-molecular-weight oligomers (19),  $\text{Zn}^{2+}$ -A $\beta$ 40 oligomers, or mixtures of the two preparations at 9:1, or 4:1 concentration ratio (Fig. 3). Ten  $\mu\text{M}$   $\text{Zn}^{2+}$ -free A $\beta$ 40 displayed a rapid increase in ThT fluorescence in serum-free culture medium. The linear part of the fluorescence curve had a slope of  $0.81 \pm 0.08$  arbitrary units/h. Such a fast increase in ThT fluorescence relative to measurements in hypotonic buffers is typically observed in serum-free medium because of the relatively high concentration of  $\text{Na}^+$  and  $\text{Ca}^{2+}$  salts, which are known to accelerate A $\beta$  aggregation and fibril formation (33–36).

Seeding  $\text{Zn}^{2+}$ -free A $\beta$ 40 with 10 or 20%  $\text{Zn}^{2+}$ -A $\beta$ 40 oligomers affected both the slope and the plateau value of the ThT fluorescence. Specifically, the slopes decreased to  $0.44 \pm 0.05$  arbitrary units/h for 10% and  $0.33 \pm 0.03$  arbitrary units/h in the presence of 20%  $\text{Zn}^{2+}$ -A $\beta$ 40 oligomers, respectively. The ThT fluorescence at the plateau decreased by  $\sim 35\%$  and  $\sim 45\%$  relative to the plateau signal of A $\beta$ 40 in the presence of 10 and 20%  $\text{Zn}^{2+}$ -A $\beta$ 40 oligomers, respectively, suggesting a reduction of aligned cross- $\beta$ -sheet content. The sample containing 10  $\mu\text{M}$   $\text{Zn}^{2+}$ -A $\beta$ 40 oligomers showed little increase in ThT fluorescence relative to  $\text{Zn}^{2+}$ -free A $\beta$ 40. These data suggest that  $\text{Zn}^{2+}$ -A $\beta$ 40 oligomers attenuate the nucleation step of A $\beta$ 40 fibrillization and interfere with fibril growth. The ThT results are in agreement with TEM images presented in supplemental Figs. S3 and S4. Thus, our results indicate that not only  $\text{Zn}^{2+}$  but also  $\text{Zn}^{2+}$ -A $\beta$ 40 oligomers interfere with A $\beta$ 40 assembly.

**Metastable  $\text{Zn}^{2+}$ -A $\beta$ 40 oligomers Irreversibly Suppress Spontaneous Neuronal Activity**—The most common forms of spontaneous neuronal activity *in vivo* and *in vitro* are synchronous intracellular calcium ( $[\text{Ca}^{2+}]_i$ ) transients and bursts of action potentials in large populations of neurons involved in local circuits. Typically, in serum-free media, synchronous  $[\text{Ca}^{2+}]_i$  bursts can be recorded at stable rates and amplitudes for 2–3 h at room temperature (21, 37). To evaluate how fresh  $\text{Zn}^{2+}$ -A $\beta$ 40 oligomers affect neuronal function, we added them to primary rat hippocampal neurons in serum-free culture media



**FIGURE 4. Effect of metastable  $\text{Zn}^{2+}$ -A $\beta$ 40 oligomers on primary hippocampal neurons.** *a*, top panels, gradual rise in basal  $[\text{Ca}^{2+}]_i$  in cultured neurons. Bottom panels,  $\text{Ca}^{2+}$ -influx peaks. *b*,  $\text{Ca}^{2+}$ -imaging of the same fields after background subtraction. The y axis represents Fluo-4AM fluorescence under carefully standardized experimental conditions, including dye-loading time, temperature, light-source intensity, detector offset, and gain. *c*, net change of spontaneous  $[\text{Ca}^{2+}]_i$  bursts in the presence of A $\beta$ 40 monomers (green), A $\beta$ 40 fibrils (blue),  $\text{Zn}^{2+}$  (purple), or metastable  $\text{Zn}^{2+}$ -A $\beta$ 40 oligomers (red). Negative values are relative to the initial  $[\text{Ca}^{2+}]_i$  burst rate. *d*, resting  $[\text{Ca}^{2+}]_i$  in the same population of neurons. The y axis represents Fluo-4AM fluorescence under the same standardized conditions as in *b* and corresponds to the values of the net  $[\text{Ca}^{2+}]_i$  changes obtained after subtracting initial  $[\text{Ca}^{2+}]_i$ . *e*, viability of neurons at  $t = 72$  h measured by immunostaining for neuron-specific enolase. The data are presented as mean  $\pm$  S.E. for three independent experiments compared with the control. N.S., non-significant.

and measured spontaneous  $\text{Ca}^{2+}$  activity using the fluorescent  $\text{Ca}^{2+}$ -binding dye Fluo-4AM (38). The control conditions included freshly prepared  $\text{Zn}^{2+}$ -free A $\beta$ 40, A $\beta$ 40 fibrils, and  $\text{Zn}^{2+}$ . An additional control was MOPS (pH 6.9) diluted in serum-free cell-culture medium at the same concentration used for preparing  $\text{Zn}^{2+}$ -A $\beta$ 40 oligomers. We found that MOPS did not significantly affect the rate or the amplitude of  $\text{Ca}^{2+}$  activity or basal  $[\text{Ca}^{2+}]_i$  (data not shown).

The effect of  $\text{Zn}^{2+}$ -A $\beta$ 40 oligomers on  $\text{Ca}^{2+}$  transients in a typical field of cultured hippocampal neurons is shown in Fig. 4, *a* and *b*. Initially, the fluorescence intensity of resting  $[\text{Ca}^{2+}]_i$  was consistently below 10 relative fluorescence units. On average, 5–8 transient  $\text{Ca}^{2+}$  events per minute were measured, reaching up to 80 relative fluorescence units. After 60 min of incubation with 10  $\mu\text{M}$   $\text{Zn}^{2+}$ -A $\beta$ 40 oligomers, the mean  $\text{Ca}^{2+}$  firing rate gradually decreased to  $\sim 3$ –5  $\text{min}^{-1}$  (Fig. 4, *a* and *b*, and supplemental Fig. S5, *a* and *b*), and the net number of  $\text{Ca}^{2+}$  events was almost completely suppressed by 120 min (Fig. 4c and supplemental Fig. S5). An early indicator of neuronal damage is a gradual rise in basal  $[\text{Ca}^{2+}]_i$ . In our experiments, an

increase in  $[\text{Ca}^{2+}]_i$  was observed  $\sim 30$  min after adding freshly prepared  $\text{Zn}^{2+}$ -A $\beta$ 40 oligomers (Fig. 4, *a*, *b*, and *d*) with further increase by a factor of 4–5 by 120 min. Extensively washing out the  $\text{Zn}^{2+}$ -A $\beta$ 40 oligomers did not reverse the change in basal  $[\text{Ca}^{2+}]_i$ , nor did it affect the steady increase in the basal  $[\text{Ca}^{2+}]_i$  signal (Fig. 4d). This suggests that  $\text{Zn}^{2+}$ -A $\beta$ 40-induced alterations of cell physiology were irreversible for at least 60 min after washing.

Of all the treatment conditions, only  $\text{Zn}^{2+}$ -A $\beta$ 40 oligomers induced a marked decrease in firing rates and in resting  $[\text{Ca}^{2+}]_i$  fluorescence. Treatment with  $\text{Zn}^{2+}$ -free A $\beta$ 40 induced a slight, transient increase in the neuronal firing rate at  $\sim 10$  min (Fig. 4c) that became statistically insignificant by 30 min and completely waned after 60 min. Importantly, when the same preparations of  $\text{Zn}^{2+}$ -A $\beta$ 40 oligomers were stored for at least 16 h at room temperature before application, they did not affect spontaneous  $\text{Ca}^{2+}$  activity. TEM images of these  $\text{Zn}^{2+}$ -A $\beta$ 40 oligomer preparations revealed large amorphous aggregates extending more than 100 nm (supplemental Fig. S4), which likely formed by association of



the small quasi-spherical oligomers observed at earlier time points (Fig. 1a).

Two other  $\text{Ca}^{2+}$ -binding dyes, Fura-2AM and Oregon Green BAPTA-2AM yielded very similar results (data not shown), suggesting that the observations were unrelated to the use of Fluo-4AM.

**Metastable  $\text{Zn}^{2+}$ -A $\beta$ 40 Oligomers Cause Neuronal Death—**Alterations in neuronal activity and basal  $[\text{Ca}^{2+}]_i$  following treatment with  $\text{Zn}^{2+}$ -A $\beta$ 40 oligomers indicated neuronal dysfunction, which might lead to neuronal death. To test this prediction, we applied  $\text{Zn}^{2+}$ -A $\beta$ 40 oligomers, freshly prepared  $\text{Zn}^{2+}$ -free A $\beta$ 40, or fibrillar A $\beta$ 40 to primary hippocampal neurons and measured their viability by immunostaining for neuron-specific enolase, a standard assay for specifically detecting neuronal, rather than glial, cell death. The cell viability experiments were performed in serum-containing medium at 37 °C. We could not assess the morphology of A $\beta$ 40 under these conditions because they were indistinguishable from those of serum proteins.

In initial experiments, we added 10  $\mu\text{M}$  of each A $\beta$ 40 preparation, 10 mM MOPS, or 20  $\mu\text{M}$   $\text{Zn}^{2+}$  to the neurons and measured neuronal viability following incubation for 48 h. Under these conditions, we observed little or no toxicity induced by the  $\text{Zn}^{2+}$ -A $\beta$ 40 oligomers (supplemental Fig. S6) or any of the other conditions (data not shown).

This result was inconsistent with the toxic effect of the  $\text{Zn}^{2+}$ -A $\beta$ 40 oligomers on spontaneous  $\text{Ca}^{2+}$  activity and basal  $[\text{Ca}^{2+}]_i$  levels. A potential explanation for this apparent discrepancy was rapid self-association of the metastable  $\text{Zn}^{2+}$ -A $\beta$ 40 oligomers in serum-containing medium into large, non-toxic aggregates, similar to those shown in supplemental Fig. S4. In contrast to serum-free medium, this medium has a complex composition, including serum proteins and growth factors, which likely affect the rate of A $\beta$ 40 aggregation.

To test this hypothesis, we changed our protocol. Instead of adding 10  $\mu\text{M}$  of any A $\beta$ 40 preparation in one portion at  $t = 0$ , the same total amount of each preparation was added in four freshly prepared aliquots (2.5  $\mu\text{M}$  each) at  $t = 0, 12, 24$ , and 36 h. Remarkably, under these conditions, the  $\text{Zn}^{2+}$ -A $\beta$ 40 oligomers reduced neuronal survival by  $85\% \pm 3\%$  (Fig. 4e). In contrast, no statistically significant difference was observed between the viability of untreated neurons and those treated with MOPS buffer, A $\beta$ 40 fibrils, or 20  $\mu\text{M}$   $\text{Zn}^{2+}$ . 10  $\mu\text{M}$  A $\beta$ 40 caused  $20 \pm 8\%$  decrease in neuronal viability ( $p < 0.05$ ), in agreement with many previous observations. Overall, our results indicate that freshly prepared  $\text{Zn}^{2+}$ -A $\beta$ 40 oligomers are highly toxic to cultured neurons, induce changes in normal cellular physiology within minutes, and cause neuronal death within hours. Importantly, the apparent toxicity of  $\text{Zn}^{2+}$ -A $\beta$ 40 strongly depends on the assembly state of the metastable oligomers, giving weight to their structure-toxicity interplay (Fig. 4 and supplemental Figs. S3, S4, and S6). Although the quasi-spherical  $\text{Zn}^{2+}$ -A $\beta$ 40 assemblies ( $\varnothing = 7\text{--}15$  nm, Fig. 1) were highly toxic, their large aggregates ( $\varnothing \geq 100$  nm, supplemental Fig. S4) were benign.

## DISCUSSION

The reported results provide a detailed structure-toxicity study of early-forming, metastable, toxic  $\text{Zn}^{2+}$ -A $\beta$ 40 oligomers. Our experiments in primary hippocampal cultures showed that the small  $\text{Zn}^{2+}$ -A $\beta$ 40 oligomers inhibited spontaneous neuronal activity and caused neuronal death. Destabilization of neuronal network activity is thought to cause the cognitive impairment associated with AD (39, 40). Dysregulation of  $[\text{Ca}^{2+}]_i$  is a prominent feature of AD. It is involved both in neuronal excitotoxicity and in apoptosis (41). Our experiments in primary hippocampal neurons showed that the  $\text{Zn}^{2+}$ -A $\beta$ 40 oligomers inhibited spontaneous neuronal activity (Fig. 4, a–c), induced a time-dependent elevation in basal  $\text{Ca}^{2+}$  levels (Fig. 4d), and, at later time points, caused neuronal death (Fig. 4e). The formation of  $\text{Zn}^{2+}$ -A $\beta$ 40 oligomers may disrupt  $\text{Ca}^{2+}$  metabolism and synaptic communication, and persistent insults may contribute to neuronal apoptosis.

The small (7–15 nm)  $\text{Zn}^{2+}$ -A $\beta$ 40 assemblies have unique structural characteristics. Our TEM, AFM, CD, and x-ray diffraction data indicate that these oligomers are organized in a cross- $\beta$  arrangement typical of mature amyloid fibrils (42), yet they exhibit quasi-spherical morphologies characteristic of A $\beta$  oligomers (43). Furthermore, we show that the small quasi-spherical oligomers decrease the rate of fibril growth and, thus, may increase the steady-state concentration of toxic  $\text{Zn}^{2+}$ -free A $\beta$  forms. Our detailed structure-toxicity characterization of the  $\text{Zn}^{2+}$ -A $\beta$ 40 oligomers indicates that only the early-forming small (7–15 nm) assemblies are toxic. Upon incubation ( $\geq 16$  h), the initial  $\text{Zn}^{2+}$ -A $\beta$ 40 oligomers coalesce into larger structures (supplemental Fig. S4) and concomitantly lose their toxicity (supplemental Fig. S6). Our data provide mechanistic insights into the work of Deshpande *et al.* (11), who highlighted the role of  $\text{Zn}^{2+}$  in the formation and accumulation of toxic A $\beta$  oligomers, and of Cuajungco *et al.* (44), who observed loss of A $\beta$  toxicity upon prolonged incubation with  $\text{Zn}^{2+}$ . Though apparently,  $\text{Zn}^{2+}$  binding prevents A $\beta$  fibrillogenesis, the toxic behavior of the  $\text{Zn}^{2+}$ -A $\beta$ 40 oligomers prepared here is akin to that of  $\text{Zn}^{2+}$ -free A $\beta$  oligomers, which become less toxic upon transformation into fibrils (45, 46).

Similarly to native amylospheroids (23), toxic  $\text{Zn}^{2+}$ -A $\beta$ 40 oligomers may be considered off-pathway with regard to fibril formation (14). Other quasi-spherical toxic oligomers exhibiting  $\beta$ -sheet-rich structures have recently been reported for A $\beta$ 40 oligomers in the absence of  $\text{Zn}^{2+}$  (22). These oligomers formed following 30–60 h incubation at 4 °C. In contrast, the  $\text{Zn}^{2+}$ -A $\beta$ 40 oligomers reported here were obtained within seconds at room temperature and retained their quasi-spherical morphologies for at least 2 h in serum-free medium. It is tempting to hypothesize that  $\text{Zn}^{2+}$  binding accelerates formation of oligomers similar to those reported by Chimon *et al.* (22), although testing this hypothesis will require detailed, side-by-side comparison of the two species.

On the basis of the data obtained here, we propose a structure-kinetic model for  $\text{Zn}^{2+}$ -A $\beta$ 40 assembly spanning from the earliest metastable toxic oligomers to aged, benign morphologies (Fig. 5). Fig. 5a presents putative arrangements of  $\text{Zn}^{2+}$ -A $\beta$ 40 in mono- to multilayer assemblies rich in  $\beta$ -sheet and

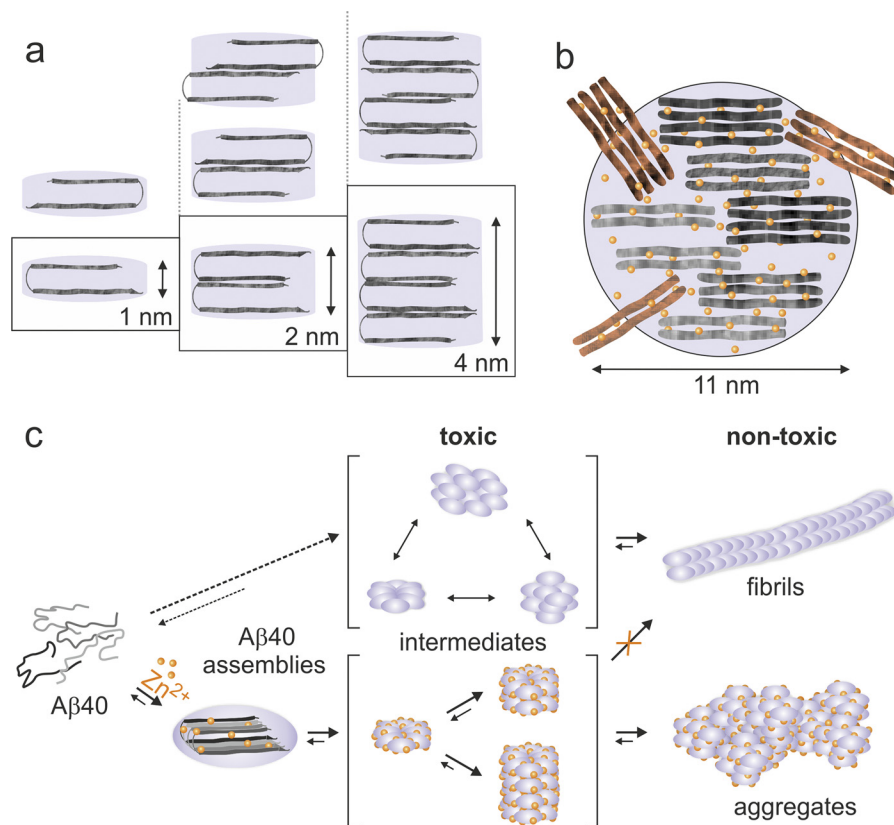


FIGURE 5. **Model of  $\text{Zn}^{2+}$ -A $\beta$ 40 oligomer structure and assembly.** *a*, A $\beta$ 40 packing in  $\text{Zn}^{2+}$ -A $\beta$ 40 viewed along the intermolecular H-bond direction. A $\beta$ 40 adopts a hairpin conformation and packs in mono-, bi-, or tetralayers. *b*, hypothetical arrangement of  $\text{Zn}^{2+}$  and A $\beta$ 40 in a toxic assembly shown perpendicular to the plane of H-bond direction. *c*, oligomerization pathways of A $\beta$ 40 in the absence (top panels) or presence of  $\text{Zn}^{2+}$  (bottom panels).

cross- $\beta$  assemblies as depicted by our CD, ThT, and x-ray diffraction analyses (Figs. 2 and 3). X-ray diffraction analysis also implies that the major conformation of A $\beta$ 40 in the aggregates resembles a hairpin, similar to the one described in A $\beta$  fibrils by Petkova *et al.* (47, 48). However, our data cannot reveal the super-structural organization of molecules (*i.e.* symmetry of organization or registry of A $\beta$ 40) in multilayered A $\beta$ 40 assemblies (Fig. 5*a*). Combined AFM and x-ray diffraction analyses showed mostly abundant monolayers as well as bilayers and tetralayers but not trilayer arrangements. We propose that monolayers have kinetic and/or thermodynamic preference for arrangement in bilayers, ultimately forming tetralayers, which may be mediated by intermolecular coordination of  $\text{Zn}^{2+}$  ions (14, 25). This may result in enhanced A $\beta$ 40 C-terminal dynamics, as reported recently (49).

We estimate a total number of 20 molecules of A $\beta$ 40 in  $\text{Zn}^{2+}$ -A $\beta$ 40 monomeric oligomers (110 Å/4.67 Å) (Fig. 5*b*), where 110 Å is the average diameter per oligomer derived from TEM (Fig. 1, *a* and *b*) and 4.67 Å is the cross- $\beta$ -sheet distance measured by x-ray powder diffraction (Fig. 2*b*). Each oligomer is composed of small crystalline assemblies of ~4 A $\beta$ 40 molecules, as indicated by the x-ray diffraction analysis. These  $\text{Zn}^{2+}$ -A $\beta$ 40 oligomers are distinct in their three-dimensional structures from analogous, toxic oligomers formed in the absence of  $\text{Zn}^{2+}$  (43). Fig. 5*c* presents a comparative scheme of A $\beta$ 40 oligomerization pathways in the presence or absence of  $\text{Zn}^{2+}$ . Metastable  $\text{Zn}^{2+}$ -A $\beta$ 40 oligomers form quasi-spherical mono-, bi-, or tetralayer toxic structures that

strongly interfere with fibril formation. Aged  $\text{Zn}^{2+}$ -A $\beta$ 40 oligomers exhibit benign activity, similar to  $\text{Zn}^{2+}$ -free A $\beta$ 40 fibrils, but differ in their morphologies.

In conclusion, our results provide quantitative structural, spectroscopic, and functional analyses of metastable and toxic  $\text{Zn}^{2+}$ -A $\beta$ 40 oligomers in cultured hippocampal neurons. We show that binding of stoichiometric  $\text{Zn}^{2+}$  concentrations modulates A $\beta$ 40 neurotoxicity via structural organization mechanisms mediated by coordination chemistry. Hence, carefully targeted,  $\text{Zn}^{2+}$ -specific chelators may be beneficial for treatment of diseases associated with A $\beta$  oligomerization (50–52).

**Acknowledgments**—The electron microscopy studies were conducted at the Irving and Cherna Moskowitz Center for Nano and Bio-Nano Imaging at the Weizmann Institute of Science.

## REFERENCES

1. Wolfe, M. S. (2003) The secretases of Alzheimer's disease. *Curr. Top. Dev. Biol.* **54**, 233–261
2. Hardy, J., and Selkoe, D. J. (2002) The amyloid hypothesis of Alzheimer's disease. Progress and problems on the road to therapeutics. *Science* **297**, 353–356
3. Selkoe, D. J. (2008) Soluble oligomers of the amyloid  $\beta$ -protein impair synaptic plasticity and behavior. *Behav. Brain Res.* **192**, 106–113
4. Heimerling, K. (2000) A unifying hypothesis of Alzheimer's disease. IV. Causation and sequence of events. *Rev. Neurosci.* **11**, 213–328
5. Klein, W. L., Stine, W. B., Jr., and Teplow, D. B. (2004) Small assemblies of unmodified amyloid  $\beta$ -protein are the proximate neurotoxin in Alzheimer's disease. *Neurobiol. Aging* **25**, 569–580



6. Lovell, M. A., Robertson, J. D., Teesdale, W. J., Campbell, J. L., and Markesbery, W. R. (1998) Copper, iron and zinc in Alzheimer's disease senile plaques. *J. Neurol. Sci.* **158**, 47–52
7. Dong, J., Atwood, C. S., Anderson, V. E., Siedlak, S. L., Smith, M. A., Perry, G., and Carey, P. R. (2003) Metal binding and oxidation of amyloid- $\beta$  within isolated senile plaque cores. Raman microscopic evidence. *Biochemistry* **42**, 2768–2773
8. Miller, L. M., Wang, Q., Telivala, T. P., Smith, R. J., Lanzirrotti, A., and Miklossy, J. (2006) Synchrotron-based infrared and X-ray imaging shows focalized accumulation of Cu and Zn co-localized with  $\beta$ -amyloid deposits in Alzheimer's disease. *J. Struct. Biol.* **155**, 30–37
9. Stoltenberg, M., Bush, A. I., Bach, Smidt, G. K., Larsen, A., Rungby, J., Lund, S., Doering, P., and Danscher, G. (2007) Amyloid plaques arise from zinc-enriched cortical layers in APP/PS1 transgenic mice and are paradoxically enlarged with dietary zinc deficiency. *J. Neurosci.* **150**, 357–369
10. Frederickson, C. J., Koh, J. Y., and Bush, A. I. (2005) The neurobiology of zinc in health and disease. *Nat. Rev. Neurosci.* **6**, 449–462
11. Deshpande, A., Kawai, H., Metherate, R., Glabe, C. G., and Busciglio, J. (2009) A role for synaptic zinc in activity-dependent A $\beta$  oligomer formation and accumulation at excitatory synapses. *J. Neurosci.* **29**, 4004–4015
12. Lee, J. Y., Cole, T. B., Palmiter, R. D., Suh, S. W., and Koh, J. Y. (2002) Contribution by synaptic zinc to the gender-disparate plaque formation in human Swedish mutant APP transgenic mice. *Proc. Natl. Acad. Sci. U.S.A.* **99**, 7705–7710
13. Bush, A. I., Pettingell, W. H., Multhaup, G., d Paradis, M., Vonsattel, J. P., Gusella, J. F., Beyreuther, K., Masters, C. L., and Tanzi, R. E. (1994) Rapid induction of Alzheimer A  $\beta$  amyloid formation by zinc. *Science* **265**, 1464–1467
14. Noy, D., Solomonov, I., Sinkevich, O., Arad, T., Kjaer, K., and Sagi, I. (2008) Zinc-amyloid  $\beta$  interactions on a millisecond time-scale stabilize non-fibrillar Alzheimer-related species. *J. Am. Chem. Soc.* **130**, 1376–1383
15. Garai, K., Sengupta, P., Sahoo, B., and Maiti, S. (2006) Selective destabilization of soluble amyloid  $\beta$  oligomers by divalent metal ions. *Biochem. Biophys. Res. Commun.* **345**, 210–215
16. Huang, X., Atwood, C. S., Moir, R. D., Hartshorn, M. A., Vonsattel, J. P., Tanzi, R. E., and Bush, A. I. (1997) Zinc-induced Alzheimer's A $\beta$ 1–40 aggregation is mediated by conformational factors. *J. Biol. Chem.* **272**, 26464–26470
17. Kodali, R., Williams, A. D., Chemuru, S., and Wetzel, R. (2010) A $\beta$ (1–40) forms five distinct amyloid structures whose  $\beta$ -sheet contents and fibril stabilities are correlated. *J. Mol. Biol.* **401**, 503–517
18. Chen, W. T., Liao, Y. H., Yu, H. M., Cheng, I. H., and Chen, Y. R. (2011) Distinct effects of  $\text{Zn}^{2+}$ ,  $\text{Cu}^{2+}$ ,  $\text{Fe}^{3+}$ , and  $\text{Al}^{3+}$  on amyloid- $\beta$  stability, oligomerization, and aggregation. Amyloid- $\beta$  destabilization promotes annular protofibril formation. *J. Biol. Chem.* **286**, 9646–9656
19. Bitan, G., Vollers, S. S., and Teplow, D. B. (2003) Elucidation of primary structure elements controlling early amyloid  $\beta$ -protein oligomerization. *J. Biol. Chem.* **278**, 34882–34889
20. Papa, M., Bundman, M. C., Greenberger, V., and Segal, M. (1995) Morphological analysis of dendritic spine development in primary cultures of hippocampal neurons. *J. Neurosci.* **15**, 1–11
21. Eilers, J., Schneggenburger, R., and Konnerth, A. (1995) In *Single Channel Recording* (Sakmann, B., and Neher, E., eds) pp. 213–229, Plenum Press, New York
22. Chimon, S., Shaibat, M. A., Jones, C. R., Calero, D. C., Aizezi, B., and Ishii, Y. (2007) Evidence of fibril-like  $\beta$ -sheet structures in a neurotoxic amyloid intermediate of Alzheimer's  $\beta$ -amyloid. *Nat. Struct. Mol. Biol.* **14**, 1157–1164
23. Hoshi, M., Sato, M., Matsumoto, S., Noguchi, A., Yasutake, K., Yoshida, N., and Sato, K. (2003) Spherical aggregates of  $\beta$ -amyloid (amylospheroid) show high neurotoxicity and activate tau protein kinase I/glycogen synthase kinase-3 $\beta$ . *Proc. Natl. Acad. Sci. U.S.A.* **100**, 6370–6375
24. Ono, K., Condrón, M. M., and Teplow, D. B. (2009) Structure-neurotoxicity relationships of amyloid  $\beta$ -protein oligomers. *Proc. Natl. Acad. Sci. U.S.A.* **106**, 14745–14750
25. Miller, Y., Ma, B., and Nussinov, R. (2010) Zinc ions promote Alzheimer A $\beta$  aggregation via population shift of polymorphic states. *Proc. Natl. Acad. Sci. U.S.A.* **107**, 9490–9495
26. Glenner, G. G., Eanes, E. D., Bladen, H. A., Linke, R. P., and Termine, J. D. (1974)  $\beta$ -Pleated sheet fibrils. A comparison of native amyloid with synthetic protein fibrils. *J. Histochem. Cytochem.* **22**, 1141–1158
27. Kirschner, D. A., Inouye, H., Duffy, L. K., Sinclair, A., Lind, M., and Selkoe, D. J. (1987) Synthetic peptide homologous to  $\beta$  protein from Alzheimer disease forms amyloid-like fibrils *in vitro*. *Proc. Natl. Acad. Sci. U.S.A.* **84**, 6953–6957
28. Malinchik, S. B., Inouye, H., Szumowski, K. E., and Kirschner, D. A. (1998) Structural analysis of Alzheimer's  $\beta$ (1–40) amyloid. Protofilament assembly of tubular fibrils. *Biophys. J.* **74**, 537–545
29. Sachse, C., Fändrich, M., and Grigorieff, N. (2008) Paired  $\beta$ -sheet structure of an A $\beta$ (1–40) amyloid fibril revealed by electron microscopy. *Proc. Natl. Acad. Sci. U.S.A.* **105**, 7462–7466
30. Jahn, T. R., Makin, O. S., Morris, K. L., Marshall, K. E., Tian, P., Sikorski, P., and Serpell, L. C. (2010) The common architecture of cross- $\beta$  amyloid. *J. Mol. Biol.* **395**, 717–727
31. LeVine, H., 3rd. (1993) Thioflavine T interaction with synthetic Alzheimer's disease  $\beta$ -amyloid peptides. Detection of amyloid aggregation in solution. *Protein Sci.* **2**, 404–410
32. Bernstein, S. L., Dupuis, N. F., Lazo, N. D., Wyttenbach, T., Condrón, M. M., Bitan, G., Teplow, D. B., Shea, J. E., Ruotolo, B. T., Robinson, C. V., and Bowers, M. T. (2009) Amyloid- $\beta$  protein oligomerization and the importance of tetramers and dodecamers in the aetiology of Alzheimer's disease. *Nat. Chem.* **1**, 326–331
33. Stine, W. B., Jr., Dahlgren, K. N., Krafft, G. A., and LaDu, M. J. (2003) *In vitro* characterization of conditions for amyloid- $\beta$  peptide oligomerization and fibrillogenesis. *J. Biol. Chem.* **278**, 11612–11622
34. Nichols, M. R., Moss, M. A., Reed, D. K., Lin, W. L., Mukhopadhyay, R., Hoh, J. H., and Rosenberry, T. L. (2002) Growth of  $\beta$ -amyloid(1–40) protofibrils by monomer elongation and lateral association. Characterization of distinct products by light scattering and atomic force microscopy. *Biochemistry* **41**, 6115–6127
35. Isaacs, A. M., Senn, D. B., Yuan, M., Shine, J. P., and Yankner, B. A. (2006) Acceleration of amyloid  $\beta$ -peptide aggregation by physiological concentrations of calcium. *J. Biol. Chem.* **281**, 27916–27923
36. Itkin, A., Dupres, V., Dufrène, Y. F., Bechinger, B., Ruyschaert, J. M., and Raussens, V. (2011) Calcium ions promote formation of amyloid  $\beta$ -peptide (1–40) oligomers causally implicated in neuronal toxicity of Alzheimer's disease. *PLoS ONE* **6**, e18250
37. Neher, E. (2011) In *Imaging: A Laboratory Manual* (Rafael, Y., ed) pp. 417–426, Cold Spring Harbor Laboratory Press, Cold Spring Harbor, NY
38. Khazipov, R., Esclapez, M., Caillard, O., Bernard, C., Khalilov, I., Tyzio, R., Hirsch, J., Dzhalal, V., Berger, B., and Ben-Ari, Y. (2001) Early development of neuronal activity in the primate hippocampus *in utero*. *J. Neurosci.* **21**, 9770–9781
39. Palop, J. J., Chin, J., and Mucke, L. (2006) A network dysfunction perspective on neurodegenerative diseases. *Nature* **443**, 768–773
40. Uhlhaas, P. J., and Singer, W. (2006) Neural synchrony in brain disorders. Relevance for cognitive dysfunctions and pathophysiology. *Neuron* **52**, 155–168
41. LaFerla, F. M. (2002) Calcium dyshomeostasis and intracellular signalling in Alzheimer's disease. *Nat. Rev. Neurosci.* **3**, 862–872
42. Serpell, L. C. (2000) Alzheimer's amyloid fibrils. Structure and assembly. *Biochim. Biophys. Acta* **1502**, 16–30
43. Rahimi, F., Shanmugam, A., and Bitan, G. (2008) Structure-function relationships of pre-fibrillar protein assemblies in Alzheimer's disease and related disorders. *Curr. Alzheimer Res.* **5**, 319–341
44. Cuajungco, M. P., Goldstein, L. E., Nunomura, A., Smith, M. A., Lim, J. T., Atwood, C. S., Huang, X., Farrag, Y. W., Perry, G., and Bush, A. I. (2000) Evidence that the  $\beta$ -Amyloid Plaques of Alzheimer's Disease Represent the Redox-silencing and Entombment of A $\beta$  by Zinc. *J. Biol. Chem.* **275**, 19439–19442
45. Dahlgren, K. N., Manelli, A. M., Stine, W. B., Jr., Baker, L. K., Krafft, G. A., and LaDu, M. J. (2002) Oligomeric and fibrillar species of amyloid- $\beta$  peptides differentially affect neuronal viability. *J. Biol. Chem.* **277**, 32046–32053
46. Klein, W. L., Krafft, G. A., Finch, C. E. (2001) Targeting small A $\beta$  oligomers. The solution to an Alzheimer's disease conundrum? *Trends Neuro-*

## Structure-Toxicity Interplay of $\text{Zn}^{2+}$ -A $\beta$ 40 Oligomers

- sci.* **24**, 219–224
47. Petkova, A. T., Ishii, Y., Balbach, J. J., Antzutkin, O. N., Leapman, R. D., Delaglio, F., and Tycko, R. (2002) A structural model for Alzheimer's  $\beta$ -amyloid fibrils based on experimental constraints from solid-state NMR. *Proc. Natl. Acad. Sci. U.S.A.* **99**, 16742–16747
48. Tycko, R. (2011) Solid-state NMR studies of amyloid fibril structure. *Annu. Rev. Phys. Chem.* **62**, 279–299
49. Rezaei-Ghaleh, N., Giller, K., Becker, S., and Zweckstetter, M. (2011) Effect of zinc binding on  $\beta$ -amyloid structure and dynamics: implications for A $\beta$  aggregation. *Biophys. J.* **101**, 1202–1211
50. Cherny, R. A., Legg, J. T., McLean, C. A., Fairlie, D. P., Huang, X., Atwood, C. S., Beyreuther, K., Tanzi, R. E., Masters, C. L., and Bush, A. I. (1999) Aqueous dissolution of Alzheimer's disease A $\beta$  amyloid deposits by bio-metal depletion. *J. Biol. Chem.* **274**, 23223–23228
51. Adlard, P. A., Cherny, R. A., Finkelstein, D. I., Gautier, E., Robb, E., Cortes, M., Volitakis, I., Liu, X., Smith, J. P., Perez, K., Laughton, K., Li, Q. X., Charman, S. A., Nicolazzo, J. A., Wilkins, S., Deleva, K., Lynch, T., Kok, G., Ritchie, C. W., Tanzi, R. E., Cappai, R., and Masters, C. L., Barnham, K. J., and Bush, A. I. (2008) Rapid restoration of cognition in Alzheimer's transgenic mice with 8-hydroxy quinoline analogs is associated with decreased interstitial A $\beta$ . *Neuron* **59**, 43–55
52. Faux, N. G., Ritchie, C. W., Gunn, A., Rembach, A., Tsatsanis, A., Bedo, J., Harrison, J., Lannfelt, L., Blennow, K., Zetterberg, H., Ingelsson, M., Masters, C. L., Tanzi, R. E., Cummings, J. L., Herd, C. M., and Bush, A. I. (2010) PBT2 rapidly improves cognition in Alzheimer's Disease. Additional phase II analyses. *J. Alzheimers Dis.* **20**, 509–516

Supporting Information for

***Zn<sup>2+</sup>-A $\beta$ 40 complexes form metastable quasi-spherical oligomers that are cytotoxic to cultured hippocampal neurons \****

**Inna Solomonov<sup>1,2,#</sup>, Eduard Korkotian<sup>3,#</sup>, Benjamin Born<sup>1,2</sup>, Yishay Feldman<sup>4</sup>, Arkady Bitler<sup>4</sup>,  
Farid Rahimi<sup>5</sup>, Huiyuan Li<sup>5</sup>, Gal Bitan<sup>5,6,7</sup>, and Irit Sagi<sup>1,2</sup>**

<sup>1</sup>From the Department of Structural Biology and <sup>2</sup>Department of Biological Regulation,

<sup>3</sup>Department of Neurobiology, and <sup>4</sup>Department of Chemical Research Support, the Weizmann Institute of Science, Rehovot 76100, Israel; <sup>5</sup>Department of Neurology, David Geffen School of Medicine, <sup>6</sup>Brain Research Institute, and <sup>7</sup>Molecular Biology Institute, University of California at Los Angeles, Los Angeles, CA 90095, USA

<sup>#</sup>equal contribution



## Transmission electron microscopy (TEM) images

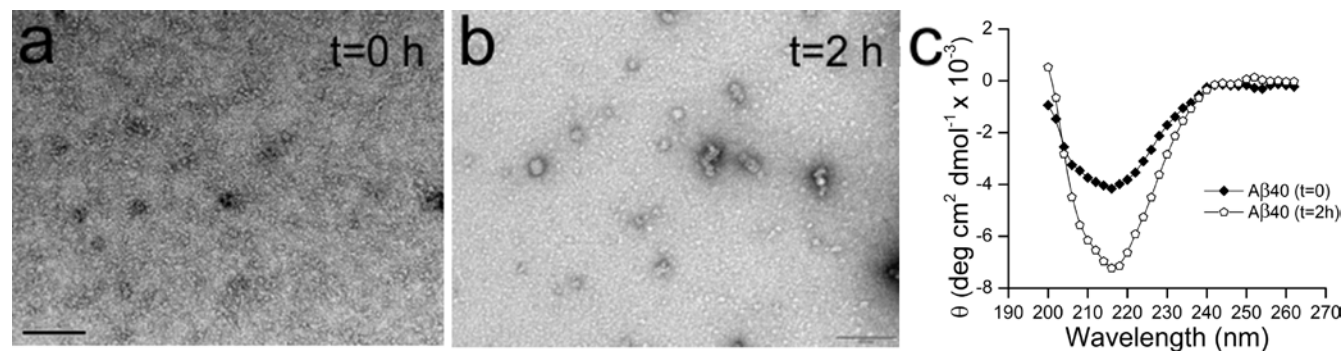


Figure S1. TEM images of Zn<sup>2+</sup>-free Aβ<sub>40</sub> preparations a) at  $t = 0$  and b)  $t = 2$  h, respectively, in serum-free culture media. The scale bar corresponds to 100 nm. c) CD spectra of Zn<sup>2+</sup>-free Aβ<sub>40</sub> at  $t = 0$  and at  $t = 2$  h.

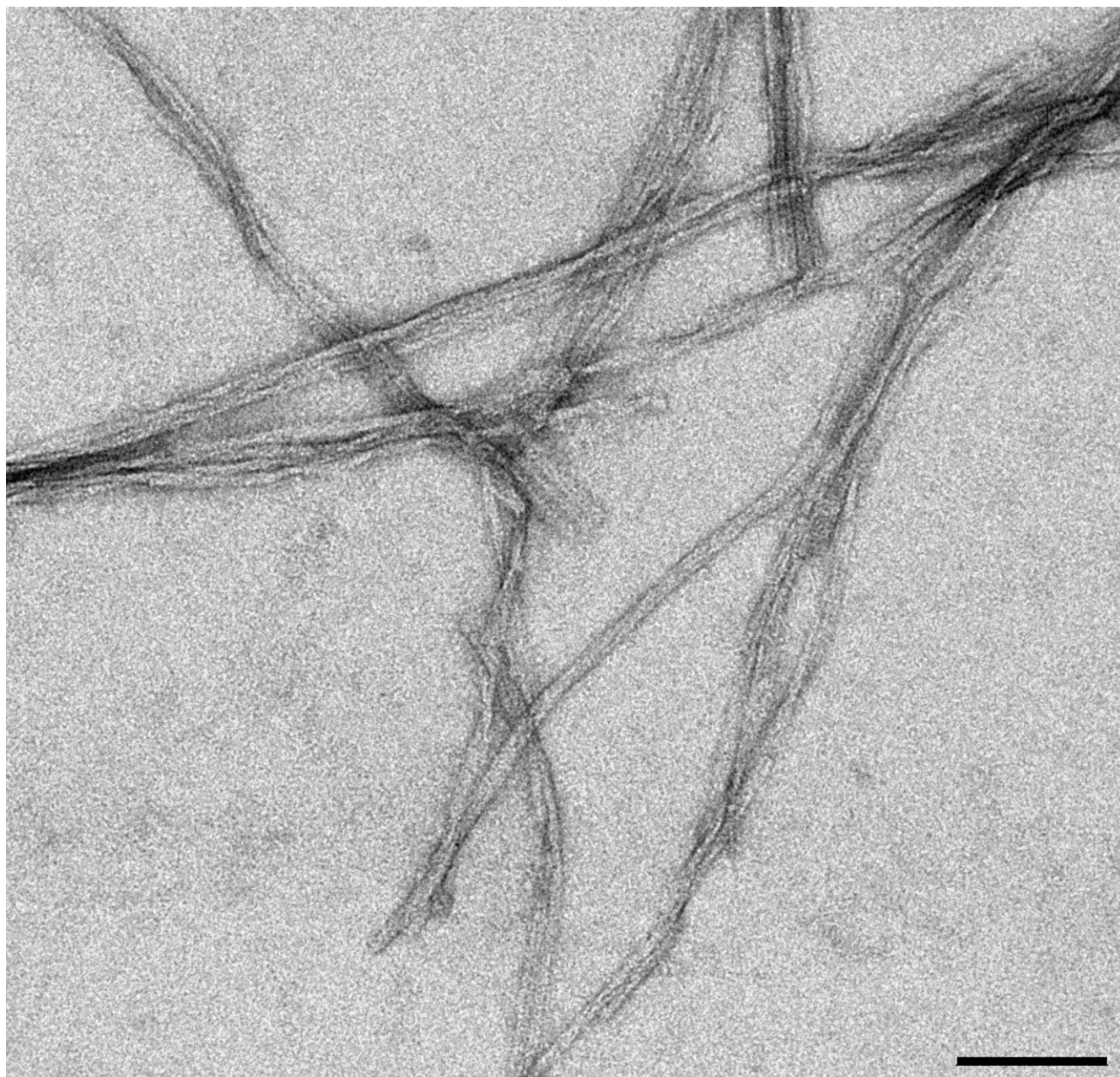


Figure S2. A representative TEM image of A $\beta$ 40 fibrils grown in MOPS. Before addition to neuronal cultures, the fibril suspensions were sonicated for 20 s, centrifuged for 20 min at 2000 $\times$ g, and washed three times in 10 mM MOPS buffer. The scale bar corresponds to 100 nm.

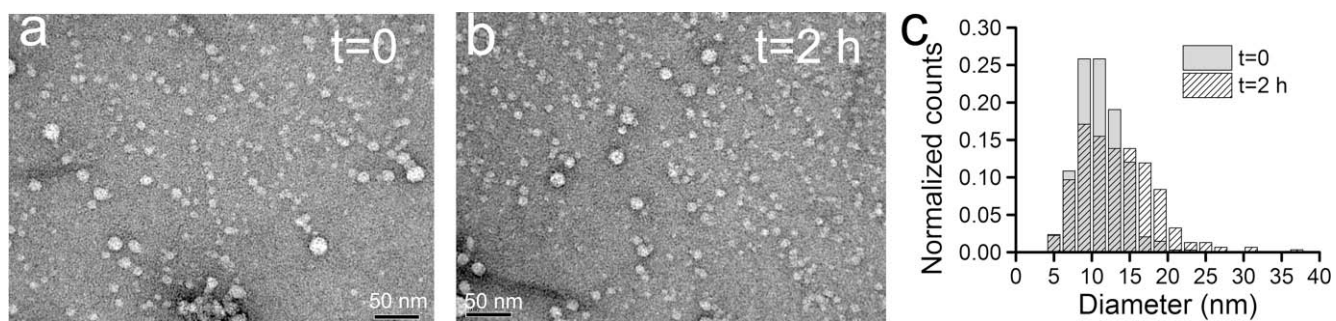


Figure S3: TEM images of metastable  $Zn^{2+}$ -A $\beta$ 40 oligomers in serum-free cell-culture medium at a)  $t = 0$  and b)  $t = 2$  h. c) Diameter distributions of metastable  $Zn^{2+}$ -A $\beta$ 40 oligomers.



**TEM image of  $Zn^{2+}$ -A $\beta$ 40**

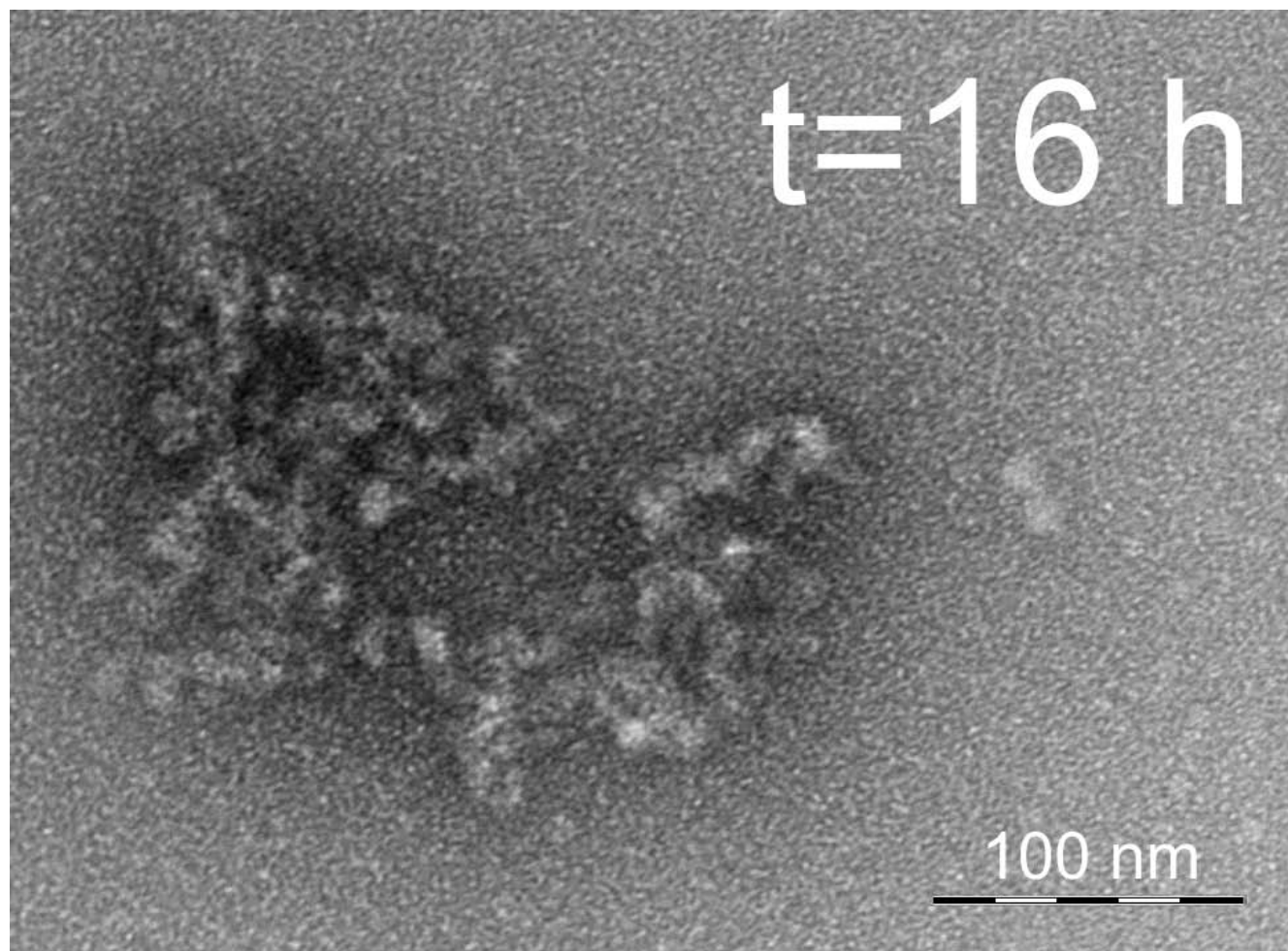


Figure S4. TEM image of  $Zn^{2+}$ -A $\beta$ 40 oligomers aged in MOPS buffer (pH 6.9) before addition to neuron cultures.

# Intracellular $\text{Ca}^{2+}$ imaging

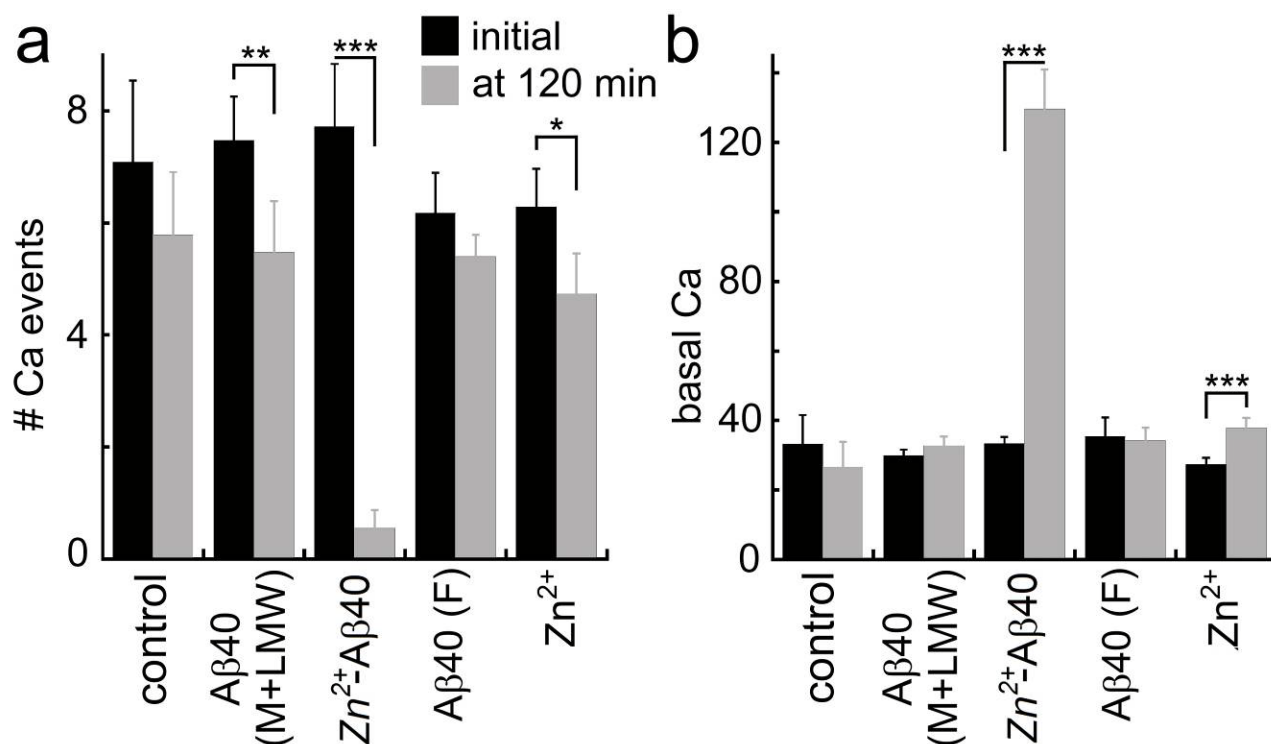


Figure S5. Absolute number of a) spontaneous  $\text{Ca}^{2+}$  events and of b) basal intracellular  $\text{Ca}^{2+}$  levels. “Aβ40 (M+LMW)” and “Aβ40 (F)” correspond to  $\text{Zn}^{2+}$ -free Aβ40 (a mixture of monomers and low molecular weight oligomers) and fibrillar Aβ40, respectively. \* $p < 0.05$ , \*\* $p < 0.01$ , \*\*\* $p < 0.001$  relative to  $t = 0$  ( $t$ -test). Note moderate reduction of spontaneous events (a) and the restricted yet statistically significant increase of basal calcium levels (b) the following free  $\text{Zn}^{2+}$  application. Such changes have not been associated with cell viability decrease at long-term stages. Aβ40 (M+LMW) did not change basal calcium, though it reduced spontaneous neuronal activity (a) and cell viability (Fig 4e in the main manuscript).

## Cell-viability analysis

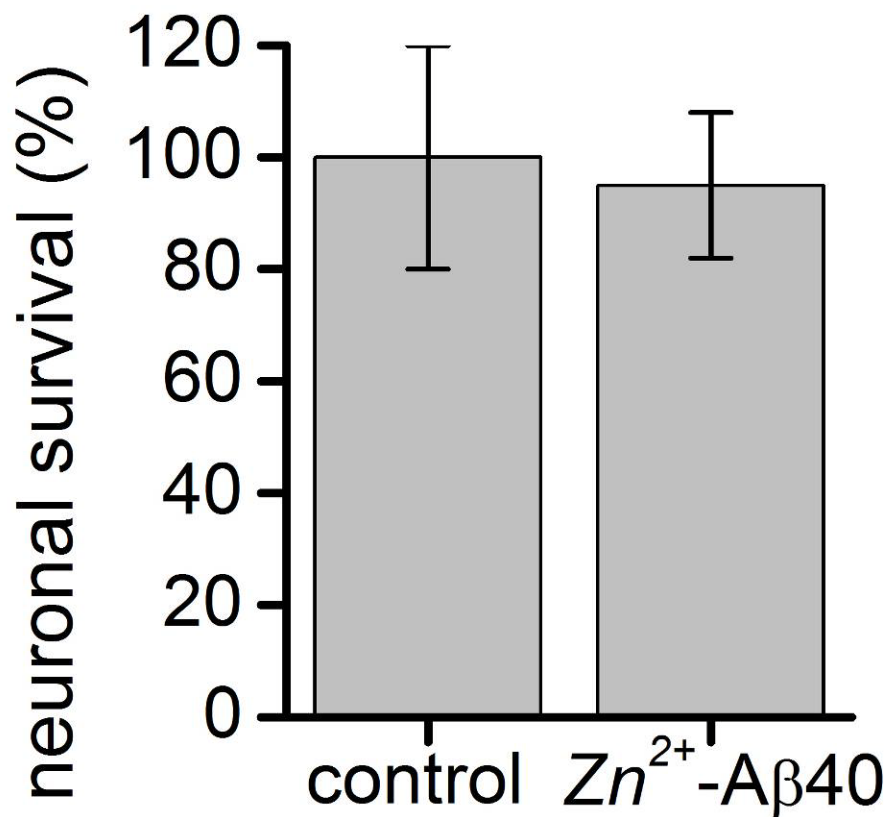


Figure S6. Effect of 10  $\mu$ M  $Zn^{2+}$ -A $\beta$ 40 oligomers on the viability of primary hippocampal neurons. Toxicity was not observed, presumably because of relatively rapid self-association of the initial, small, toxic oligomers into large, non-toxic assemblies at 37 °C in serum-containing media.